CONF-930722--3

LA-UR- 93-1798

Title: TERRESTRIAL MAGNETOSPHERIC IMAGING: NUMERICAL MODELING OF LOW ENERGY NEUTRAL ATOMS

Author(s): Kurt R. Moore, SST-7
Herbert O. Funsten, SST-7
DAvid J. McComas, SST-7
EArl E. Scime, SST-7
Michelle F. Thomsen, SST-7

Submitted to: 1993 SPIE CONFERENCE 2008 INSTRUMENTATION FOR MAGNETOSPHERIC IMAGERY II, SAN DIEGO, CA
11-16 JULY 1993

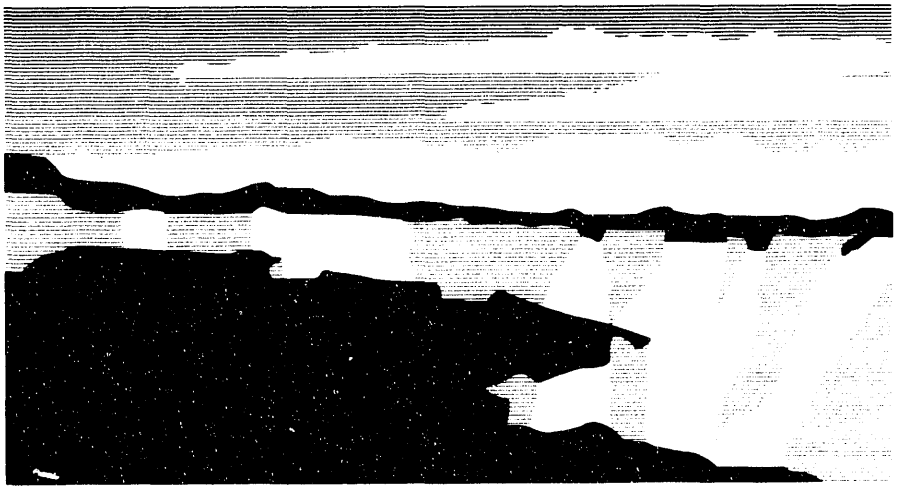

Los Alamos
NATIONAL LABORATORY

Terrestrial Magnetospheric Imaging: Numerical Modeling of Low Energy Neutral Atoms

Kurt R. Moore
Herbert O. Funsten
David J. McComas
Earl E. Scime
Michelle F. Thomsen

Los Alamos National Laboratory
SST-7 / D466
Los Alamos, NM 87545

ABSTRACT

Imaging of the terrestrial magnetosphere can be performed by detection of low energy neutral atoms (LENAs) that are produced by charge exchange between magnetospheric plasma ions and cold neutral atoms of the Earth's geocorona. As a result of recent instrumentation advances[1-5] it is now feasible to make energy-resolved measurements of LENAs from less than 1 keV to greater than 30 keV. To model expected LENA fluxes at a spacecraft, we initially used a simplistic, spherically symmetric magnetospheric plasma model.[6] We now present improved calculations of both hydrogen and oxygen line-of-sight LENA fluxes expected on orbit for various plasma regimes as predicted by the Rice University Magnetospheric Specification Model. We also estimate expected image count rates based on realistic instrument geometric factors, energy passbands, and image accumulation intervals. The results indicate that presently proposed LENA instruments are capable of imaging of storm time ring current and potentially even quiet time ring current fluxes, and that phenomena such as ion injections from the tail and subsequent drifts toward the dayside magnetopause may also be deduced.

1. INTRODUCTION

Energetic neutral atoms (ENAs) and low energy neutral atoms (LENAs) are produced by charge exchange of magnetospheric plasma with cold neutral atoms (predominantly hydrogen) of the Earth's geocorona. ENAs can be used to globally image the Earth's ring current at energies greater than approximately 30 keV.[7-11] The high energy ring current, however, is only one component in the complicated terrestrial magnetospheric plasma environment. The majority of magnetospheric plasma is less energetic. Recently reported instrumentation advances[1-5] provide techniques for LENA imaging in the energy range of <1 keV to >30 keV. These energies are characteristic of plasma populations such as the low energy ring current and the plasma sheet. Here we investigate the feasibility of LENA imaging the low energy ring current during different geomagnetic conditions.

We previously reported[6] results from a numerical model, patterned after the pioneering work of Roelof[7], which calculates line of sight LENA fluxes expected on orbit for various plasma regimes according to:

$$f_i(E) = \sigma_{iH} \int_l J_i(\underline{r},E,\alpha)\, n_H(\underline{r})\, dl. \qquad (1)$$

Using only the dominant geocoronal species, H, the LENA flux $f_i(E)$ (in units of $[cm^2\ s\ sr\ keV]^{-1}$) of atomic species i is a function of the energy-dependent charge exchange cross section σ_{iH} for the interaction $i^+ + H \rightarrow i + H^+$ (in the magnetosphere, i is dominantly either H^+ or O^+); the

magnetospheric ion flux $J_i(\underline{r},E,\alpha)$ (units of $[cm^2\ s\ sr\ keV]^{-1}$) as a function of location $\underline{r}$ in the magnetosphere, ion energy E, and pitch angle α relative to the local magnetic field; and the geocoronal neutral hydrogen number density $n_H(\underline{r})$ (units of cm^{-3}). The integral is performed over the entire line of sight path l.

Encouraged by our preliminary modeling results[6], we have extended our original numerical code. The model neutral geocoronal hydrogen number density remains a spherically symmetric isothermal Chamberlain model[13] fit to ultraviolet imaging photometer data from Dynamics Explorer 1, with 1050^o K temperature, a 500 km exobase, an exobase density of $4.4 \times 10^4\ cm^{-3}$, and a satellite critical level of 3.0 times the exobase radius.[14] The charge exchange cross sections σ_{iH} are now based on Chebyshev polynomial fits to available cross section data.[15, 16] For $H^+ + H \rightarrow H + H^+$, the cross section (in cm^2) at energy E (in keV) is given by:

$$\sigma_{HH} = 10^A, \text{ where } A = -2.384\times10^{-6}\,E^3 + 3.121\times10^{-4}\,E^2 - 0.03507\,E - 14.77 \quad (2)$$

while for $O^+ + H \rightarrow O + H^+$,

$$\sigma_{OH} = 10^B, \text{ where } B = -2.275\times10^{-6}\,E^3 + 3.070\times10^{-4}\,E^2 - 0.01630\,E - 14.98 \quad (3)$$

These cross sections are plotted in Figure 1.

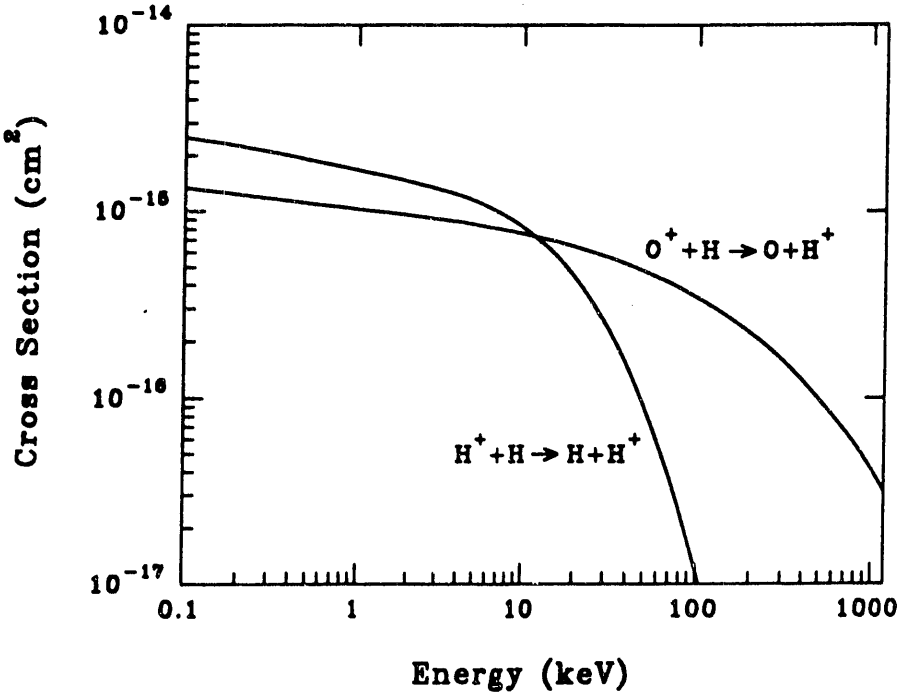

Figure 1. - Model charge exchange cross sections.

The most significant change in the simulation is in the calculation of the plasma ion flux $J_i(\underline{r},E,\alpha)$ in (1). For the preliminary model[6], we used a simple and computationally efficient empirical model of the magnetosphere to calculate $J_i(\underline{r},E,\alpha)$. We have replaced this simple magnetospheric model with the much more sophisticated but more computationally intensive Rice University Magnetospheric Specification Model (MSM).[12] This change allows us to estimate LENA signatures associated with a much wider variety of magnetospheric conditions than was previously possible. In particular, realistic LENA fluxes and corresponding instrument count rates resulting from changes in the ring current and near-Earth plasma sheet as a function of storm and substorm phases can be calculated.

The MSM predicts $J_i(\underline{r},E,\alpha)$ by determining the flux in the equatorial plane at the point that is magnetically linked (using the MSM model magnetic field) to each point in space, $\underline{r}$. The fluxes are assumed to be isotropic, removing the pitch angle dependency α. Thus, the ion flux is constant along the model magnetic field lines (not shown). Under these approximations, it is sufficient to display 2-dimensional equatorial ion flux maps rather than 3-dimensional ion flux surfaces. MSM plasma fluxes are available for protons and O^+ ions at several different times during the geomagnetic storm period of 21-23 April 1988. This period included a major geomagnetic storm and at least one magnetic substorm. We display MSM 3 keV equatorial proton fluxes for three selected but physically unrelated times in Figure 2. From top to bottom, the panels represent magnetospheric conditions during quiet time, substorm expansion phase onset, and post main phase of a geomagnetic storm. The modeled region extends to 9 R_E (90% of the nominal magnetopause standoff distance) on the dayside, 14 R_E on the flanks, and 20 R_E down the tail. The irregular boundary is an artifact of the routine used to create the plots and has no physical significance.

Enhanced proton fluxes seen as darkened regions in the nightside of the middle and bottom panels of Figure 2 are due primarily to injection of plasma sheet ions into the low energy ring current. These 3 keV ions drift both eastward and westward as they move toward the dayside. At higher energies, ion drifts become predominantly westward. Figure 3 displays MSM equatorial fluxes for 14 keV protons.

The O^+ number density in the magnetosphere can vary by an order of magnitude during magnetic storms.[17] The 14 keV MSM equatorial O^+ fluxes shown in Figure 4 are plotted on the same scale as Figures 2 and 3 and clearly show how O^+ ions injected from the near tail drift sunward to populate the ring current during this storm period. Finer temporal resolution (not shown) also reveals that the O^+ ions likewise drift in the same westward sense as the 14 keV protons of Figure 3.

A LENA imager at a given energy does not provide equatorial ion flux maps as shown in Figures 2-4 but instead measures the convolution of the 3-dimensional ion flux and the neutral geocorona, integrated along the line of sight, as indicated by (1). Two important questions for LENA imaging that we can address using our updated model are:
(1) are the count rates for a realizable instrument based on these predicted fluxes significant ?
(2) are magnetospheric phenomena such as ion injections, ring current enhancements, and ion drifts observable with a LENA imager?

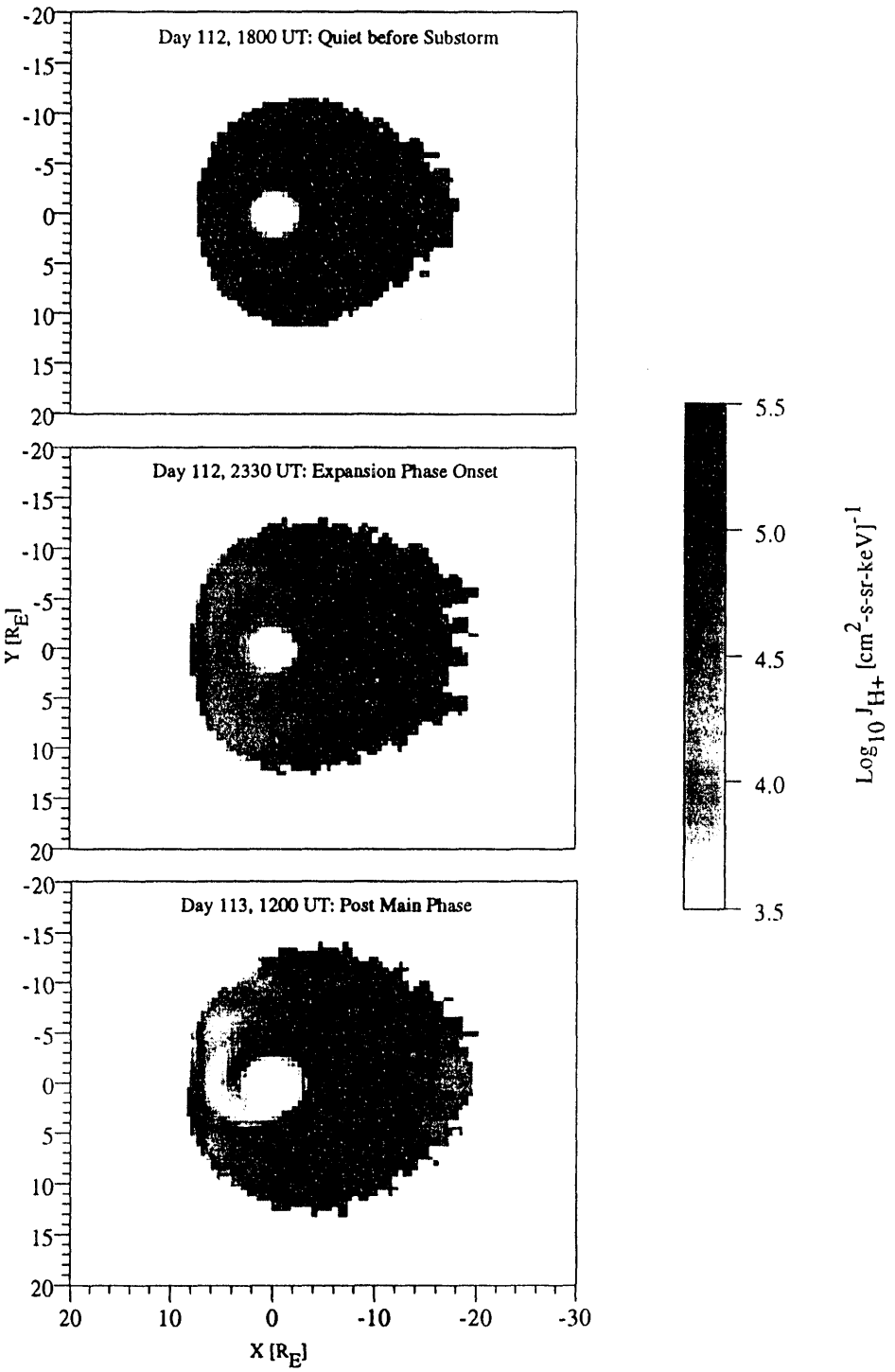

Figure 2. - MSM equatorial fluxes of 3 keV protons.

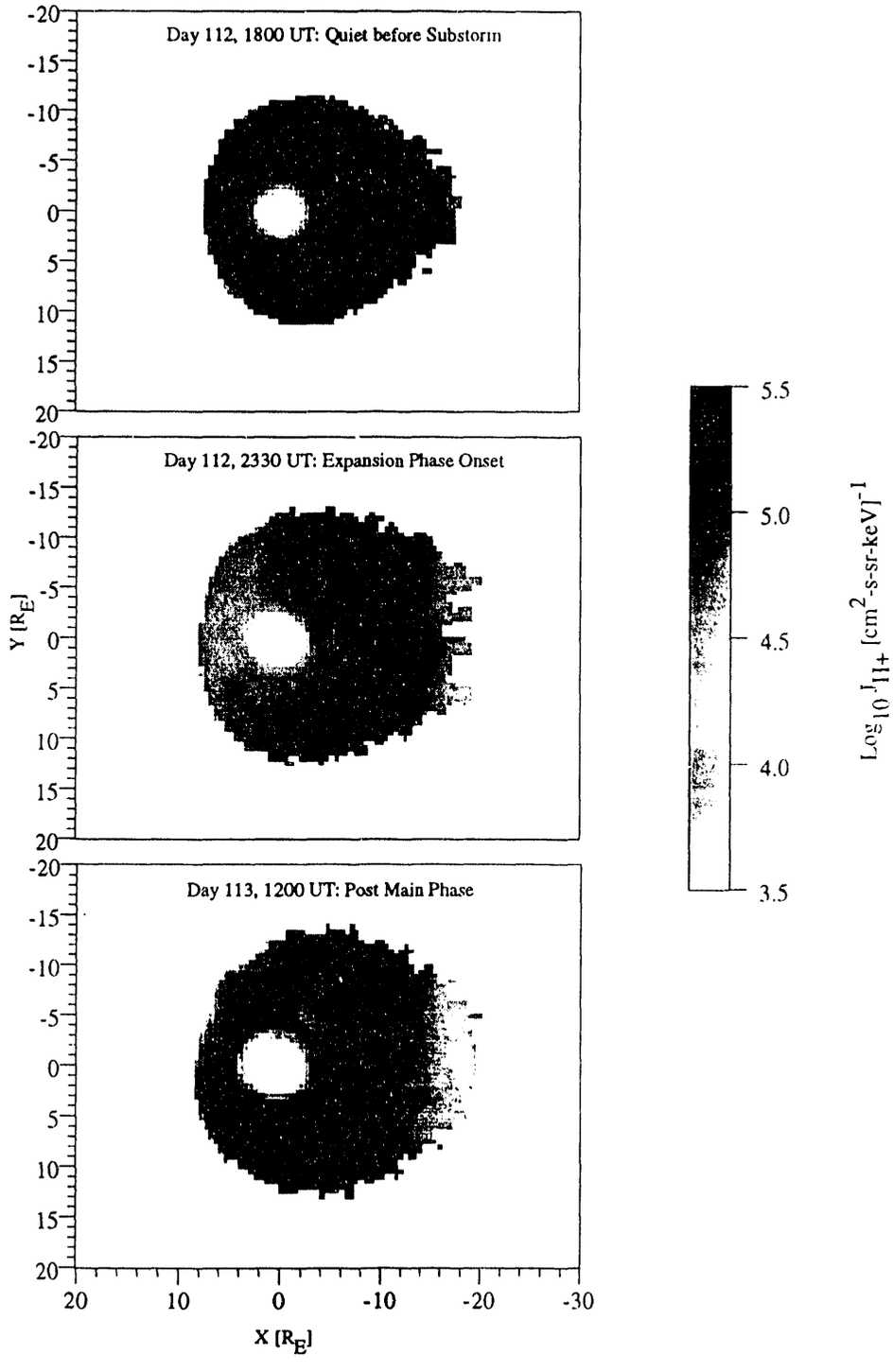

Figure 3. - MSM equatorial fluxes of 14 keV protons.

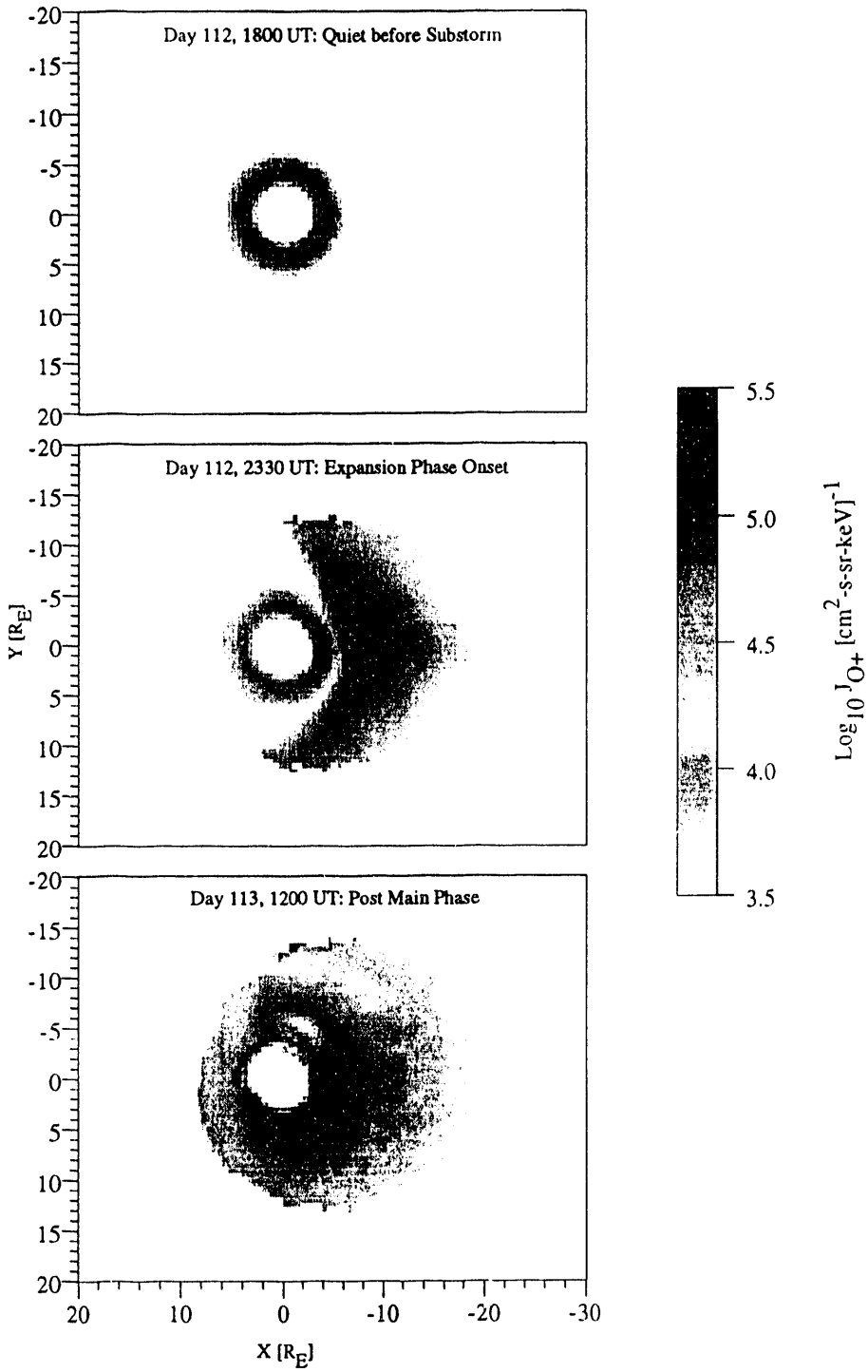

Figure 4. - MSM equatorial fluxes of 14 keV O^+ ions.

2. MODEL RESULTS

The output of the LENA simulation is an array of neutral particle fluxes as a function of look direction. The polar angle is measured relative to the local (spacecraft) Z direction and the azimuthal angle is measured relative to the local X axis (positive toward the Y axis). The local X axis always points directly away from the Earth and the local Z axis is in the plane containing the spacecraft location and the magnetic dipole axis. The result is that the Earth always appears at a polar angle of 90^{o} and an azimuthal angle of 180^{o} in these plots.

The model outputs can be plotted as images in polar and azimuthal angle space, with a coded flux color or grayscale. Images with $4^{o} \times 4^{o}$ resolution for 3 keV hydrogen at a spacecraft position of 9 R_E directly above the Earth's north pole at the same three times as Figure 2 are shown in Figure 5. Comparison of Figures 5 and 2 reveals that, despite the effects of line-of-sight integration and convolution with the geocorona, LENA signatures of the injection of protons from the tail and the sunward drifting of these protons to fill the ring current are significant.

Figure 6 shows the LENA model predictions for 14 keV hydrogen that result from the proton flux distributions shown in Figure 3. The vantage point and angular resolution are identical to Figure 5. Again, the injection of protons from the plasma sheet into the ring current is visible in the LENA flux. Also note that the westward drift observed in the MSM fluxes of Figure 3 is also evident in the bottom two LENA images of Figure 6.

The 14 keV oxygen fluxes resulting from O^{+} ions modeled in Figure 4 are displayed in Figure 7. The neutral oxygen fluxes on day 113 are comparable to the neutral hydrogen fluxes at the same time, and the westward drift of the O^{+} ions produces a similar signature in the neutral oxygen flux.

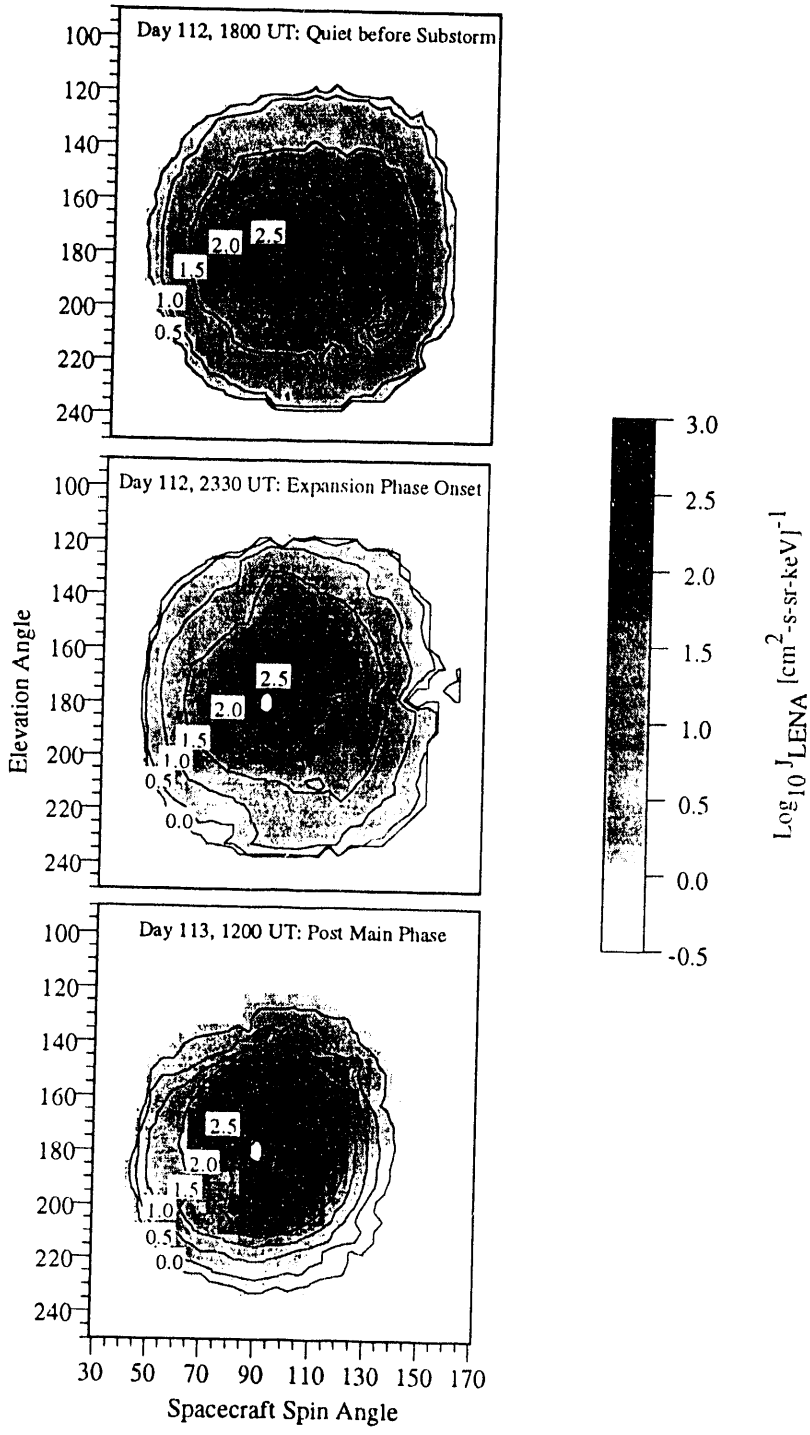

Figure 5. - Predicted line-of-sight 3 keV hydrogen LENA fluxes from 9 R_E above the North Pole.

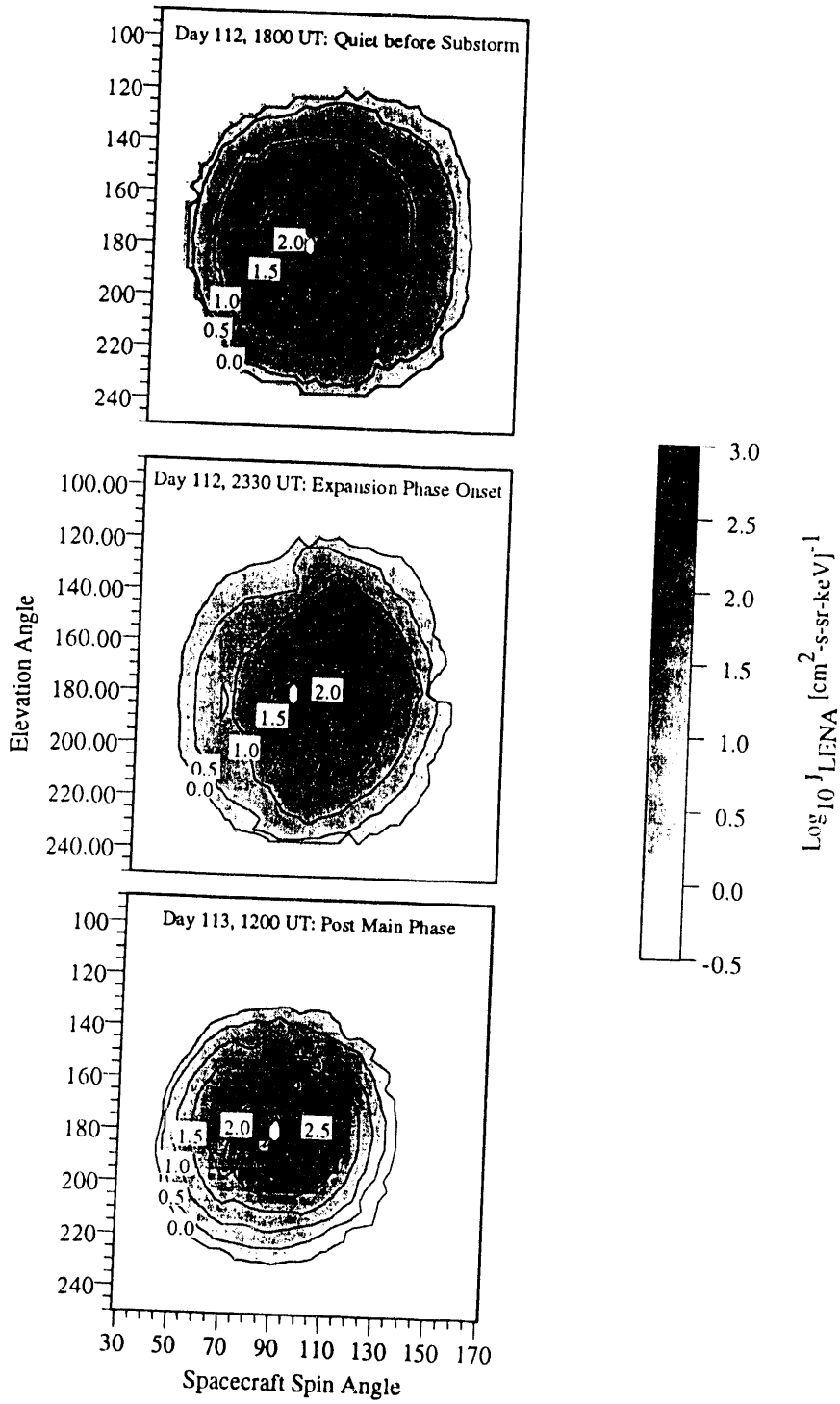

Figure 6. - Predicted line-of-sight 14 keV hydrogen LENA fluxes from 9 R_E above the North Pole.

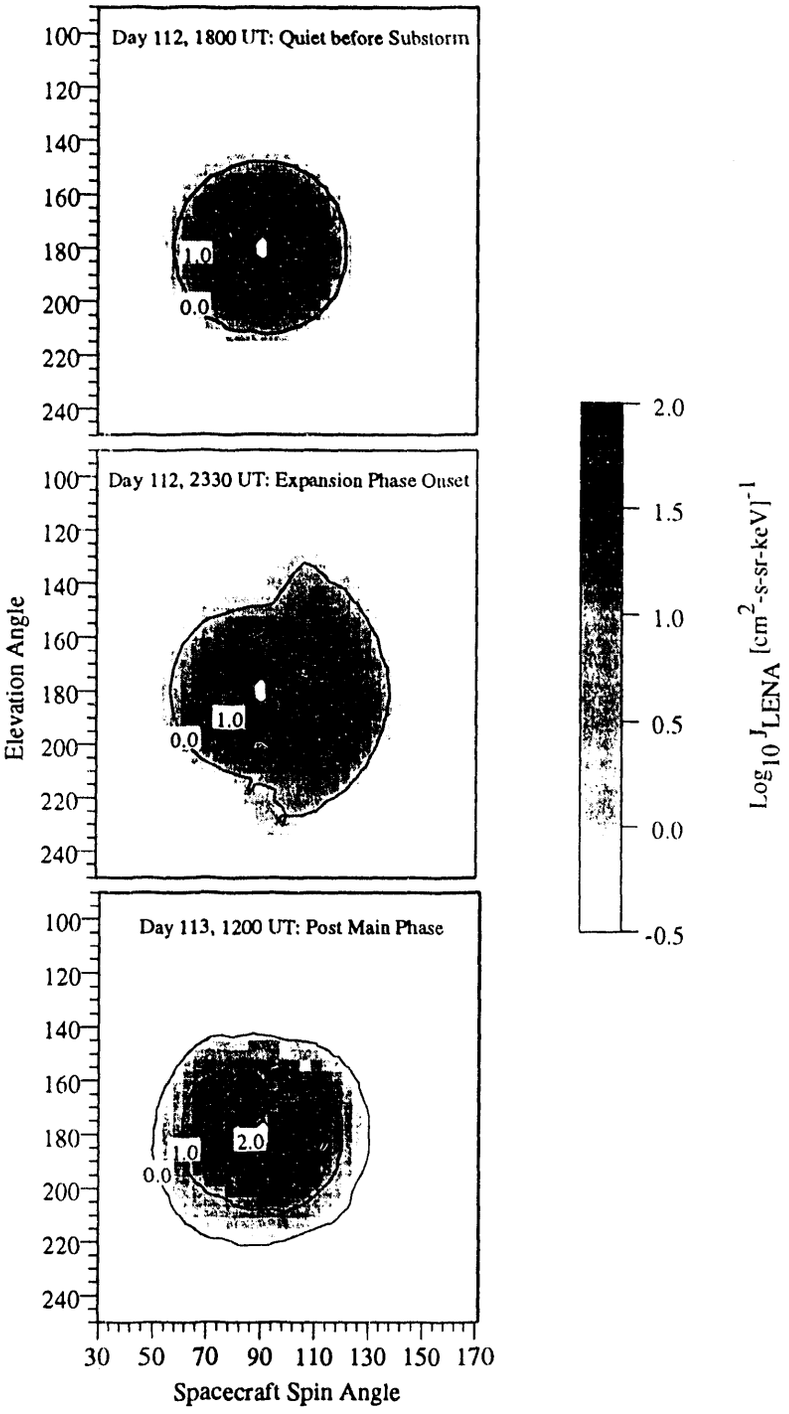

Figure 7. - Predicted line-of-sight 14 keV oxygen LENA fluxes from 9 R_E above the North Pole.

3. DISCUSSION

We present results from an improved numerical model that calculates LENA fluxes expected at a polar orbiting spacecraft. We have based our calculations on the Rice University MSM proton and O^+ fluxes and have updated our charge exchange cross sections to produce the most accurate estimates of LENA fluxes that can be made at the present time. The final step is to convert these neutral fluxes to estimates of the actual instrument count rates.

The counts expected in each pixel of LENA images can be scaled from the fluxes presented in Figures 5-7. The counts in a pixel are related to the LENA flux J_{LENA} by the relation

$$C = J_{LENA} \times E \times G \times \Delta t \qquad (4)$$

where G is the per pixel geometric factor [units of cm^2 sr eV/eV] and Δt is the observation interval. Whole instrument geometric factors for small, simple LENA imagers are 0.01-0.1 cm^2 sr eV/eV while a full scale imager such as that intended for NASA's Inner Magnetosphere Imager (IMI) mission could achieve ~1 cm^2 sr eV/eV.[2,3] The commensurate per pixel geometric factor is ~0.02 cm^2 sr eV/eV for a 10^o x 10^o pixel [3] or ~0.003 cm^2 sr eV/eV for 4^o x 4^o pixels. The observation interval is based on the total accumulation time, fraction of a spin that the instrument is looking in a given direction, and the number of sequential energy bands to be sampled. For example, if these values are 5 minutes (300 s), 2 x $4^o/360^o$ = 0.022, and 1/4 = 0.25, respectively, then Δt = 1.67 s. Thus, for the 14 keV hydrogen image (Figure 6), the counts per pixel would be 0.07 J_{LENA} and the 1 count level would be approximately the 1.0 contour.

It is clear that it is desirable to develop LENA imagers with geometric factors as large as possible, with potentially big scientific returns. Many important space physics issues will be addressed by a global LENA imager of sufficient resolution and sensitivity. Changes in ring current fluxes such as enhancements during a magnetic storm, injections of plasma sheet ions, and global ion drift patterns as a function of energy can be observed via LENA imaging on time scales as short as a few minutes. Separate imaging of hydrogen and oxygen LENAs could quantify global compositional changes in the ring current. Such global information on ring current fluxes and composition would be a valuable addition to the existing body of space data.

The results of our modeling indicate that LENA imaging of the ring current is potentially feasible but would rely on large instrument geometric factors. The scientific gains from such measurements would be immediate and significant. More simulations are currently being performed to obtain basic information necessary for LENA instrumentation and scientific development. In addition, we are continuing to investigate optimal orbit parameters for imaging other magnetospheric phenomena as well as the viability of magnetospheric tomography using multiple spacecraft. Finally, we are exploring the use of massively parallel computers to reduce the computational time per image to a sufficiently small value for real time extraction of magnetospheric parameters from LENA images.

5. ACKNOWLEDGEMENTS

We thank R. W. Spiro and R. A. Wolf for providing the MSM results. Development of the MSM at Rice University was supported by Air Force contract F19628-90-K-0012 and scientific application of the MSM by NASA grant NAGW-1655. We also thank Rick Elphic of the Los Alamos Space and Atmospheric Physics Group for invaluable discussions, support, and enthusiasm. This work was carried out under the auspices of the United States Department of Energy.

6. REFERENCES

1. D. J. McComas, B. L. Barraclough, R. C. Elphic, H. O. Funsten III, and M. F. Thomsen, "Magnetospheric Imaging With Low-energy Neutral Atoms", *Proc. Natl. Acad. Sci. USA*, **88**, 9598-9602, 1991

2. D. J. McComas, H. O. Funsten, J. T. Gosling, K. R. Moore, and M. F. Thomsen, Low Energy Neutral Atom Imaging, *proc. SPIE*, **1744**, 40, 1992

3. McComas SPIE 93

4. Funsten et al., this conference

5. Scime et al., this conference

6. K. R. Moore, D. J. McComas, H. O. Funsten, and M. F. Thomsen, "Low Energy Neutral Atom Imaging in the Earth's Magnetosphere: Modeling", *Proc. SPIE*, **1744**, 51, 1992

7. E. C. Roelof, D. G. Mitchell, and D. J. Williams, "Energetic Neutral Atoms (E ~ 50 keV) From the Ring Current: IMP 7/8 and ISEE 1", *J. Geophys. Res.*, **90**, 10991-11008, 1985

8. E. C. Roelof, "Energetic Neutral Atom Image From a Storm-Time Ring Current", *Geophys. Res. Lett.* , **14**, 652-655, 1987

9. R. W. McEntire and D. G. Mitchell, "Instrumentation for Global Magnetospheric Imaging via Energetic Neutral Atoms", *Geophys.. Monogr. Ser.* , **54**, 69-80, 1989

10. E. P. Keath, G.B. Andrews, A. F. Cheng, S. M. Krimigis, B. H. Mauk, D. G. Mitchell, and D. J. Williams, "Instrumentation for Energetic Neutral Atom Imaging of Magnetospheres", *Geophys. Monogr. Ser.* , **54**, 165-170, 1989

11. C. C. Curtis and K. C. Hseih, "Remote Sensing of Planetary Magnetospheres: Imaging via Energetic Neutral Atoms", *Geophys. Monogr. Ser.* , **54**, 247-251, 1989

12. B. Bales, J. Freeman, B. Hausman, R. Hilmer, R. Lambour, A. Nagai, R. Spiro, G.-H. Voight, R. Wolf, W. F. Denig, D. Hardy, M. Heinemann, N. Maynard, F. Rich, R. D. Belian, and T. Cayton, "Status of the Development of the Magnetospheric Specification and Forecast Model", accepted for publication in the Proceedings of the Solar-Terrestrial Prediction Workshop, Ottawa, Canada, May 18-22, 1992

13. J. W. Chamberlain, "Planetary Coronae and Atmospheric Evolution", *Planet. Space Sci.*, **11**, 901-960, 1963

14. R. L. Rairden, L. A. Frank, and J. D. Craven, "Geocoronal Imaging With Dynamics Explorer", *J. Geophys. Res.* , **91**, 13,613-13,630, 1986

15. C. F. Barnett, "Collisions of H, H_2, He, and Li Atoms with Atoms and Molecules", in *Atomic Data for Fusion*, Vol. 1, Rep. ORNL-6086, Oak Ridge National Laboratory, Oak Ridge, Tenn., 1990

16. R. A. Phaneuf, R. K. Janev, and M. S. Pindzola, "Collisions of Carbon and Oxygen Ions with Electrons, H, H_2, and He", in *Atomic Data for Fusion*, Vol. 5, Rep. ORNL-6090, Oak Ridge National Laboratory, Oak Ridge, Tenn., 1987

17. G. Gloeckler, B. Wilken, W. Stüdemann, F. M. Ipavich, D. Hovestadt, D. C. Hamilton, and G. Kremser, "First Composition Measurement of the Bulk of the Storm-Time Ring Current (1 to 300 keV/e) With AMPTE-CCE", *Geophys. Res. Lett.*, **12**, 325-328, 1971

END

DATE
FILMED
7/30/93